Metal−Metal Multiply-Bonded Complexes of Technetium. 3.[1] Preparation and Characterization of Phosphine Complexes of Technetium Possessing a Metal−Metal Bond Order of 3.5

F. Albert Cotton,*,[2a] Steven C. Haefner,[2a,b] and Alfred P. Sattelberger*,[2b]

Inorganic and Structural Chemistry Group (CST-3), Chemical Science and Technology Division, Los Alamos National Laboratory, Los Alamos, New Mexico 87545, and Laboratory for Molecular Structure and Bonding, Department of Chemistry, Texas A&M University, College Station, Texas 77843

Received July 11, 1995[⊗]

Two new ditechnetium complexes possessing Tc−Tc bonds with a formal bond order of 3.5 have been prepared in high yield. Mild chemical oxidation of $Tc_2Cl_4(PMe_2Ph)_4$ with ferrocenium hexafluorophosphate in acetonitrile produces $[Tc_2Cl_4(PMe_2Ph)_4][PF_6]$ (**1**) in 82% yield. One-electron oxidation of $Tc_2Cl_4(PMe_2Ph)_4$ by ferrocenium hexafluorophosphate in the presence of ppnCl (ppn = bis(triphenylphosphine)iminium) yielded the neutral compound $Tc_2Cl_5(PMe_2Ph)_3$ (**2**) in 89% yield. Both species are paramagnetic, as evidenced by EPR spectroscopy, and possess a $\sigma^2\pi^4\delta^2\delta^*$ ground state electronic configuration on the basis of structural and spectroscopic data. The solid state structures of three forms of **1** have been investigated by X-ray crystallography together with the structure of **2**. The crystallographic parameters for these structures are as follows: $[Tc_2Cl_4(PMe_2Ph)_4][PF_6]$ (**1a**, orthorhombic form), $C222_1$ with $a = 9.448(1)$ Å, $b = 24.299(1)$ Å, $c = 18.231(1)$ Å, $V = 4185.4(6)$ Å^3, and $Z = 4$; $[Tc_2Cl_4(PMe_2Ph)_4][PF_6]$ (**1b**, monoclinic form), $P2_1/n$ with $a = 12.799(4)$ Å, $b = 18.254(2)$ Å, $c = 17.945(5)$ Å, $\beta = 96.39(1)°$, $V = 4166(2)$ Å^3, and $Z = 4$; $[Tc_2Cl_4(PMe_2Ph)_4][PF_6]\cdot{}^1/_2$THF (**1**$\cdot{}^1/_2$THF), $P2_1/c$ with $a = 10.580(3)$ Å, $b = 33.327(3)$ Å, $c = 13.861(5)$ Å, $\beta = 111.04(2)°$, $V = 4562(1)$ Å^3, and $Z = 4$; $Tc_2Cl_5(PMe_2Ph)_3$ (**2**), $P2_1/c$ with $a = 11.134(1)$ Å, $b = 14.406(1)$ Å, $c = 19.501(5)$ Å, $\beta = 98.144(6)°$, $V = 3096.3(7)$ Å^3, and $Z = 4$. The cation in **1** is the 1,3,6,8-isomer, and the molecule in **2** is the 1,3,6-isomer. The Tc−Tc bond lengths for **1a**, **1b**, **1**$\cdot{}^1/_2$THF, and **2** (2.1092(9), 2.106(1), 2.1073(8), and 2.1092(4) Å, respectively) are slightly shorter than those of the corresponding $Tc_2Cl_4(PR_3)_4$ complexes, consistent with the removal of one electron from a δ^* orbital. Electrochemical studies reveal that both compounds are capable of undergoing a one-electron oxidation and a one-electron reduction to yield the respective Tc_2^{6+} and Tc_2^{4+} dinuclear cores. IR, EPR, and UV−vis spectroscopic data are presented for compounds **1** and **2.**

Introduction

While the field of metal−metal (M−M) multiple-bond chemistry as a whole has expanded at a dramatic rate in the past decade, the development of ditechnetium complexes that possess a metal−metal multiple bond has progressed more slowly.[3,4] Undoubtedly, this is largely due to the nuclear instability of ^{99}Tc, the most abundant isotope of this man-made element.[5] In an effort to correct this imbalance, we have directed our attention toward developing the chemistry of metal−metal bonded compounds of technetium. As part of our approach, we set out to prepare ditechnetium complexes with ligand sets that are known to support metal−metal bonding in a variety of different metal oxidation states. Investigations into the structural and spectroscopic consequences of addition and removal of electrons to and from the metal−metal bonding orbital manifold provide vital information concerning the electronic structure of M−M multiply-bonded compounds. A potentially useful coordination environment for our purposes is that afforded by the combination of halide and phosphine ligands. The ability of this type of ligand set to stabilize multiple oxidation states is best illustrated by the rich redox chemistry associated with mixed halide−phosphine complexes of Re_2^{n+} ($n = 4, 5, 6$).[3] Our previous work in the area of metal−metal multiply-bonded complexes of Tc had established a high-yield synthetic route to the preparation of $Tc_2Cl_4(PR_3)_4$ (PR_3 = PEt_3, $P(n\text{-}Pr)_3$, PMe_2Ph, and $PMePh_2$) compounds.[1a] These species represent the first examples of discrete ditechnetium complexes that possess an electron-rich triple bond. While we have been successful at exploiting $Tc_2Cl_4(PR_3)_4$ type complexes as precursors to new metal−metal bonded ditechnetium compounds,[1b] our primary goal in preparing such compounds was to investigate their redox behavior. Herein, we describe the chemical oxidation of $Tc_2Cl_4(PMe_2Ph)_4$ to produce mixed-valent Tc_2^{5+} species containing a Tc−Tc bond with a formal bond order of 3.5. The effects of removal of an electron from the δ^* orbital on the structural and spectroscopic properties of the Tc_2 core are presented.

Experimental Section

General Considerations. *Caution!* The isotope ^{99}Tc is a low-energy β-emitter ($E_{max} = 0.29$ MeV) with a half-life of 2.1×10^5 years. All manipulations were carried out in laboratories approved for low-level radioactive materials following procedures and techniques described elsewhere.[6] Ammonium pertechnetate was obtained from Oak Ridge National Laboratory and was purified as described previously.[7] $Tc_2Cl_4(PMe_2Ph)_4$ was prepared from $TcCl_4(PMe_2Ph)_2$ following the literature procedure.[1a] $[Cp_2Fe][PF_6]$ was prepared according to the

⊗ Abstract published in *Advance ACS Abstracts,* February 15, 1996.

(1) (a) Part 1: Burns, C. J.; Burrell, A. K.; Cotton, F. A.; Haefner, S. C.; Sattelberger, A. P. *Inorg. Chem.* **1994**, *33*, 2257. (b) Part 2: Bryan, J. C.; Cotton, F. A.; Daniels, L. M.; Haefner, S. C.; Sattelberger, A. P. *Inorg. Chem.* **1995**, *34*, 1875.
(2) (a) Texas A&M University. (b) Los Alamos National Laboratory.
(3) Cotton, F. A.; Walton, R. A. *Multiple Bonds Between Metal Atoms*, 2nd ed.; Oxford University Press: New York, 1993, and references cited therein.
(4) Spitsyn, V. I.; Kuzina, A. F.; Oblova, A. A.; Kryuchkov, S. V. *Russ. Chem. Rev. (Engl. Transl.)* **1985**, *54*, 373.
(5) Baldas, J. *Adv. Inorg. Chem.* **1994**, *41*, 1.

0020-1669/96/1335-1831$12.00/0

Table 1. Crystallographic Data for $[Tc_2Cl_4(PMe_2Ph)_4][PF_6]$ (**1a**, **1b**, **1**·$^1/_2$THF) and $Tc_2Cl_5(PMe_2Ph)_3$ (**2**)

	1a	**1b**	**1**·$^1/_2$THF	**2**
formula	$C_{32}H_{44}Cl_4F_6P_5Tc_2$	$C_{32}H_{44}Cl_4F_6P_5Tc_2$	$C_{34}H_{48}Cl_4F_6O_{0.5}P_5Tc_2$	$C_{24}H_{33}Cl_5P_3Tc_2$
fw	1035.32	1035.32	1071.37	787.66
space group	$C222_1$	$P2_1/n$	$P2_1/c$	$P2_1/c$
a, Å	9.448(1)	12.799(4)	10.580(3)	11.134(1)
b, Å	24.299(1)	18.254(2)	33.327(3)	14.406(1)
c, Å	18.231(1)	17.945(5)	13.861(5)	19.501(5)
β, deg		96.39(1)	111.04(2)	98.144(6)
V, Å^3	4185.4(6)	4166(2)	4562(1)	3096.3(7)
Z	4	4	4	4
ρ_{calc}, g/cm^3	1.643	1.651	1.560	1.690
μ, cm^{-1}	99.64 (Cu Kα)	11.62 (Mo Kα)	91.71 (Cu Kα)	14.93 (Mo Kα)
transm coeff., max − min	1.00−0.80	1.00−0.86	1.00−0.61	1.00−0.75
radiation (monochromated in incident beam)	Cu Kα ($\lambda_{K\alpha}$ = 1.541 84)	Mo Kα ($\lambda_{K\alpha}$ = 0.710 73)	Cu Kα ($\lambda_{K\alpha}$ = 1.541 84)	Mo Kα ($\lambda_{K\alpha}$ = 0.710 73)
temp, °C	22 ± 2	22 ± 2	22 ± 2	22 ± 2
$R(F_o)^a$ ($F_o^2 > 2\sigma(F_o^2)$)	0.031	0.049	0.050	0.026
$R_w(F_o^2)^{b,c}$ ($F_o^2 > 2\sigma(F_o^2)$)	0.081	0.124	0.141	0.066
quality-of-fit-indicator^{c,d}	1.10	1.02	1.08	1.10

^{a} $R = \sum||F_o| - |F_c||/\sum|F_o|$. ^{b} $R_w = [\sum[w(F_o^2 - F_c^2)^2]/\sum[w(F_o^2)^2]]^{1/2}$. ^{c} Weight $= 1/[\sigma(F_o^2)^2 + (aP)^2 + (bP)]$, where $P = [\max(F_o^2,0) + 2F_c^2]/3$. ^{d} Quality of fit $= [\sum[w(F_o^2 - F_c^2)^2]/(N_{obs} - N_{params})]^{1/2}$, based on all data.

method described by Gray et al.[8] Toluene, hexanes, heptane, THF (tetrahydrofuran), and diethyl ether were distilled under N_2 from either sodium or sodium/potassium alloy. Acetonitrile and methylene chloride were distilled under N_2 from CaH_2. Other reagents were purchased from commercial sources and used without further purification.

Synthetic Procedures. Unless noted otherwise, the transfer of air-sensitive solids and the work-up of air-sensitive reaction mixtures were carried out within the confines of a Vacuum Atmospheres Co. glovebox equipped with a high-capacity purification system and a Dri-Cold freezer maintained at −40 °C.

$[Tc_2Cl_4(PMe_2Ph)_4][PF_6]$·$^1/_2$THF (1·$^1/_2$THF). $Tc_2Cl_4(PMe_2Ph)_4$ (0.10 g, 0.11 mmol) was suspended in 2 mL of CH_3CN. A solution of $[Cp_2Fe][PF_6]$ (0.04 g, 0.11 mmol) in 1 mL of CH_3CN was slowly added dropwise to this suspension. Immediately, the reaction solution became dark green as $Tc_2Cl_4(PMe_2Ph)_4$ dissolved. After 15 min of stirring, 10−15 mL of a 5:1 mixture of diethyl ether and THF was added dropwise to the solution, resulting in the precipitation of a green crystalline product. The solution was cooled to −40 °C, and the green product was filtered off. The solid was then washed repeatedly with copious amounts of diethyl ether and dried under vacuum; yield 0.095 g (81%). IR (Nujol, KBr, cm^{-1}): 1434 s, 1415 m, 1342 w, 1313 w, 1295 m, 1282 m, 1198 w, 1161 w, 1103 m, 1066 w, 1030 w, 1001 w, 948 m, 909 s, 875 m, 834 s, 745 s, 692 s, 557 s, 486 s, 418 s. Electronic absorption spectrum (CH_3CN; λ_{max}, nm (ϵ, M^{-1}cm^{-1})): 1417 (2140), 586 (350), 467 (340). Anal. Calcd for $C_{34}H_{48}Cl_4F_6O_{0.5}P_5Tc_2$: C, 38.12; H, 4.52. Found: C, 38.58; H, 3.87.

$Tc_2Cl_5(PMe_2Ph)_3$ (2). $Tc_2Cl_4(PMe_2Ph)_4$ (0.20 g, 0.22 mmol) and $[Cp_2Fe][PF_6]$ (0.08 g, 0.22 mmol) were dissolved in 2 mL of CH_3CN, producing a dark green solution. After 10 min of stirring, a solution of ppnCl (0.128 g, 0.22 mmol) in 1 mL of CH_3CN was added to the reaction mixture, producing an orange precipitate. After 1 h of stirring, the orange product was collected by filtration. The solid was washed with 3 × 3 mL of CH_3CN and 3 × 3 mL of diethyl ether and then dried under vacuum; yield 0.156 g (89%). IR (Nujol, KBr, cm^{-1}): 1486 m, 1430 s, 1412 m, 1288 m, 1278 m, 1194 w, 1156 w, 1102 m, 1075 w, 1027 w, 1000 w, 949 m, 907 s, 874 w, 844 w, 741 s, 712 w, 689 s, 484 s, 416 s. Electronic absorption spectrum (CH_2Cl_2); λ_{max}, nm (ϵ, M^{-1}cm^{-1})): 1405 (1950), 728 (30), 520 (280), 445 (1250), 395 (850). Anal. Calcd for $C_{24}H_{33}Cl_5P_3Tc_2$: C, 36.60; H, 4.22. Found: C, 36.08; H, 3.29.

Physical Measurements. Electronic absorption spectra were measured on a Perkin-Elmer lambda 9 UV−vis/near-IR spectrophotometer. Electrochemical measurements were performed on an EG&G Princeton Applied Research Model 273 potentiostat. Cyclic voltammetry experiments were carried out at room temperature in CH_3CN using 0.1 M [n-Bu$_4$N][BF$_4$] as a supporting electrolyte. A platinum disk working electrode and a platinum wire counter electrode were used in conjunction with a silver wire quasi-reference electrode that was separated from the bulk solution by a fine porosity glass frit. $E_{1/2}$ values, determined as $(E_{p,a} + E_{p,c})/2$, are reported relative to an internal ferrocene standard. X-band EPR spectra were recorded as frozen solutions on a Bruker ER200D spectrometer operating at a frequency of 9.53 GHz. Elemental analyses were obtained on a Perkin-Elmer 2400 analyzer.

Table 2. Selected Atomic Coordinates and Equivalent Isotropic Displacement Parameters (Å^2) for $[Tc_2Cl_4(PMe_2Ph)_4][PF_6]$ (**1a**)

	x	y	z	U(eq)^a
Tc	0.9085(1)	0.5399(1)	0.0228(1)	0.032(1)
Cl(1)	1.0770(2)	0.5431(1)	0.1167(1)	0.053(1)
Cl(2)	0.7402(2)	0.5922(1)	−0.0386(1)	0.058(1)
P(1)	0.7330(2)	0.5379(1)	0.1241(1)	0.047(1)
P(2)	1.0834(2)	0.5947(1)	−0.0485(1)	0.048(1)

^{a} Equivalent isotropic U_{eq} is defined as one-third of the trace of the orthogonalized $\mathbf{U}_{ij}$ tensor.

X-ray Crystallographic Procedures. Crystallographic data for $[Tc_2Cl_4(PMe_2Ph)_4][PF_6]$ (**1a** and **1b**), $[Tc_2Cl_4(PMe_2Ph)_4][PF_6]$·$^1/_2$THF (**1**·$^1/_2$THF), and $Tc_2Cl_5(PMe_2Ph)_3$ (**2**) were collected following well-established procedures that have been fully described elsewhere.[9] All calculations were performed on a local area VMS cluster at Texas A&M University employing a VAX/VMS 5.5-2 computer. Data were corrected for Lorentz and polarization effects. Structure refinement was carried out using SHELXL-93.[10] Crystallographic parameters and basic information pertaining to data collection and structure refinement are summarized in Table 1. A listing of important positional and isotropic displacement parameters for **1a**, **1b**, **1**·$^1/_2$THF, and **2** are presented in Tables 2−5. Tables of anisotropic displacement parameters as well as complete tables of bond distances and angles are available as Supplementary Information.

$[Tc_2Cl_4(PMe_2Ph)_4][PF_6]$ (1a). Dark green crystals of **1a** were grown by slow evaporation of a solution of $[Tc_2Cl_4(PMe_2Ph)_4][PF_6]$ in a mixture of CH_2Cl_2/heptane. A crystal with the approximate dimensions 0.30 × 0.30 × 0.25 mm^3 was selected and fastened to the tip of a glass fiber with epoxy cement. Data collection was performed on a Rigaku AFC5R diffractometer equipped with a rotating Cu radiation source ($\lambda_{Cu\ K\alpha}$ = 1.541 84 Å) at ambient temperature. Cell parameters consistent with a face-centered orthorhombic lattice were obtained by

(6) Bryan, J. C.; Burrell, A. K.; Miller, M. M.; Smith, W. H.; Burns, C. J.; Sattelberger, A. P. *Polyhedron* **1993**, *12*, 1769, and references cited therein.
(7) Libson, K.; Barnett, B. L.; Deutsch, E. *Inorg. Chem.* **1983**, *22*, 1695.
(8) Hendrickson, D. N.; Sohn, Y. S.; Gray, H. B. *Inorg. Chem.* **1971**, *10*, 1559.
(9) (a) Bino, A.; Cotton, F. A.; Fanwick, P. E. *Inorg. Chem.* **1979**, *18*, 3558. (b) Cotton, F. A.; Frenz, B. A.; Deganello, G.; Shaver, A. *J. Organomet. Chem.* **1979**, *50*, 227.
(10) Sheldrick, G. M. SHELXL-93; Institut für Anorganische Chemie der Universität Göttingen, Göttingen, FRG, 1993.

Table 3. Selected Atomic Coordinates and Equivalent Isotropic Displacement Parameters (Å^2) for $[Tc_2Cl_4(PMe_2Ph)_4][PF_6]$ (**1b**)

	x	*y*	*z*	*U*(eq)[a]
Tc(1)	0.1338(1)	0.0198(1)	0.2672(1)	0.037(1)
Tc(2)	0.2831(1)	0.0605(1)	0.3083(1)	0.035(1)
Cl(1)	0.1555(2)	−0.0736(1)	0.1810(1)	0.055(1)
Cl(2)	0.0097(2)	0.0854(1)	0.3259(2)	0.057(1)
P(1)	0.0965(2)	−0.0832(1)	0.3510(2)	0.044(1)
P(2)	0.0740(2)	0.0977(2)	0.1567(2)	0.051(1)
Cl(3)	0.3398(2)	−0.0086(1)	0.4152(1)	0.050(1)
Cl(4)	0.3300(2)	0.1562(1)	0.2328(2)	0.053(1)
P(3)	0.2524(2)	0.1589(1)	0.3986(2)	0.046(1)
P(4)	0.4149(2)	−0.0073(2)	0.2423(2)	0.046(1)

[a] Equivalent isotropic U_{eq} is defined as one-third of the trace of the orthogonalized $\mathbf{U}_{ij}$ tensor.

Table 4. Selected Atomic Coordinates and Equivalent Isotropic Displacement Parameters (Å^2) for $[Tc_2Cl_4(PMe_2Ph)_4][PF_6]\cdot{}^1/_2THF$ (**1**·$^1/_2$THF)

	x	*y*	*z*	*U*(eq)[a]
Tc(1)	0.2081(1)	0.1284(1)	0.2984(1)	0.047(1)
Tc(2)	0.0735(1)	0.1748(1)	0.2998(1)	0.048(1)
Cl(1)	0.4037(2)	0.1554(1)	0.2838(2)	0.062(1)
Cl(2)	0.1099(2)	0.0673(1)	0.3159(2)	0.065(1)
Cl(3)	0.1168(2)	0.1924(1)	0.4714(2)	0.066(1)
Cl(4)	−0.0611(2)	0.1903(1)	0.1301(2)	0.071(1)
P(1)	0.3583(2)	0.1182(1)	0.4816(2)	0.057(1)
P(2)	0.1451(2)	0.1098(1)	0.1137(2)	0.061(1)
P(3)	0.1858(2)	0.2392(1)	0.2887(2)	0.059(1)
P(4)	−0.1285(2)	0.1414(1)	0.3135(2)	0.062(1)

[a] Equivalent isotropic U_{eq} is defined as one-third of the trace of the orthogonalized $\mathbf{U}_{ij}$ tensor.

Table 5. Selected Atomic Coordinates and Equivalent Isotropic Displacement Parameters (Å^2) for $Tc_2Cl_5(PMe_2Ph)_3$ (**2**)

	x	*y*	*z*	*U*(eq)[a]
Tc(1)	0.0097(1)	0.2284(1)	0.1548(1)	0.028(1)
Tc(2)	0.1915(1)	0.2295(1)	0.1356(1)	0.027(1)
Tc(1a)	0.068(1)	0.279(1)	0.1076(9)	0.053(5)
Tc(2a)	0.132(1)	0.182(1)	0.1856(9)	0.057(5)
Tc(1b)	0.071(2)	0.179(1)	0.111(1)	0.053(6)
Tc(2b)	0.135(2)	0.278(1)	0.186(1)	0.054(6)
Cl(1)	−0.1098(1)	0.2227(1)	0.0460(1)	0.055(1)
Cl(2)	−0.0548(1)	0.3823(1)	0.1645(1)	0.044(1)
Cl(3)	−0.0463(1)	0.0746(1)	0.1711(1)	0.045(1)
Cl(4)	0.3273(1)	0.2358(1)	0.2397(1)	0.041(1)
Cl(5)	0.1805(1)	0.2229(1)	0.0149(1)	0.050(1)
P(1)	0.0267(1)	0.2326(1)	0.2821(1)	0.032(1)
P(2)	0.2369(1)	0.3953(1)	0.1209(1)	0.037(1)
P(3)	0.2468(1)	0.0631(1)	0.1295(1)	0.037(1)

[a] Equivalent isotropic U_{eq} is defined as one-third of the trace of the orthogonalized $\mathbf{U}_{ij}$ tensor. The following occupancies were used for disordered atoms: Tc(1) and Tc(2), 96.7(1)%; Tc(1a) and Tc(2a), 1.81(8)%; Tc(1b) and Tc(2b), 1.46(8)%.

least-squares refinement of 25 well-centered reflections in the range $80 \le 2\theta \le 100°$. The unit cell dimensions and symmetry were confirmed by axial photography. Examination of systematic absences and intensity statistics led to the selection of the acentric space group $C222_1$. This choice was confirmed through successful least-squares refinement. Periodic monitoring of three representative reflections revealed no loss of intensity throughout the experiment. An absorption correction based on azimuthal scans of several reflections near $\chi = 90°$ was applied to the data. A total of 1767 data in the range $7 < 2\theta < 120$ were collected using a $\theta-2\theta$ scan technique. Of these data, 1720 were considered observed with $F_o^2 > 2\sigma(F_o^2)$. The position of the Tc atom was determined by direct methods.[11] The remaining non-hydrogen atoms were located from a series of alternating least-squares cycles and difference Fourier maps. After initial isotropic refinement, it was apparent that the phenyl rings of both phosphine ligands were disordered over two orientations. The phenyl ring bound to P(1) exhibited a disorder about the axis defined by the *ipso* and *para* carbon atoms, C(3) and C(6), respectively, creating two sets of positions for C(4), C(5), C(7), and C(8). The two planes of phenyl atoms make an angle of 76(1)° with respect to each other. The C−C bond distances of the two orientations were geometrically restrained to be nearly equivalent. The thermal displacement parameters of each set of disordered carbon atoms were further constrained to be equivalent. The occupancies of the disordered phenyl groups refined to values of 78-(1)% for C(4a), C(5a), C(7a), and C(8a) and 22(1)% for C(4b), C(5b), C(7b), and C(8b). The phenyl group of P(2) showed two sets of positions for the *ortho*, *meta*, and *para* carbon atoms (C(12) through C(16)). The two partially occupied sets of the phenyl rings are situated at an angle of 72(1)° with respect to each other. The carbon atoms of the primary orientation (C(12a)−C(16a)) were restrained to be coplanar with equivalent bond lengths. The carbon atoms of the secondary orientation (C(12b)−C(16b)) were constrained to fit a regular hexagon, but the C−C bond distances were allowed to shrink or expand uniformly. The thermal displacement parameters of each set of disordered carbon atoms were further constrained to be equivalent. The occupancies of the disordered phenyl groups refined to values of 61.8-(9)% for C(12a)−C(16a) and 38.2(9)% for C(12b)−C(16b). The models for both sets of disordered phenyl groups provided reasonable bond distances and angles for these groups. In addition to the disordered phenyl rings, the $[PF_6]^-$ anion, which resides on a crystallographic 2-fold axis, also exhibited a disorder about the F(1)−P(3)−F(1)′ axis. The 2-fold axis perpendicular to the P(3)−F(1) bond generates two equally occupied sets of four F atoms in the plane perpendicular to the F(1)−P(3)−F(1)′ axis. To account for the observed disorder, the site occupation factors of the equatorial F atoms, F(2) through F(5), were set to 0.50. All non-hydrogen atoms were refined with anisotropic thermal parameters. Hydrogen atoms were included at calculated positions with their thermal parameters proportional to those of the associated carbon atom. A correction for extinction was applied (refined extinction parameter $x = 0.000\ 61(4)$).[12] The absolute configuration of **1a** was established by the method described by Flack (Flack *x* parameter $= -0.02(3)$).[13] Final least-squares refinement of 218 parameters converged with *R* (based on *F*) of 0.031 and R_w (based on F^2) of 0.081.[14] The quality-of-fit based on F^2 was 1.11. The largest remaining peak in the final difference map, which was located 0.4 Å from C(12b), was 0.55 e/Å^3.

$[Tc_2Cl_4(PMe_2Ph)_4][PF_6]$ (1b). Green platelike crystals of **1b** were grown by slow diffusion of diethyl ether into a methylene chloride solution of $[Tc_2Cl_4(PMe_2Ph)_4][PF_6]$. A crystal with the approximate dimensions 0.40 × 0.25 × 0.15 mm^3 was mounted onto the tip of a glass fiber with epoxy cement. Data collection was performed on an Enraf-Nonius CAD4 diffractometer equipped with graphite monochromated Mo radiation ($\lambda_{Mo\ K\alpha} = 0.710\ 73$ Å). Unit cell parameters consistent with that of a primitive monoclinic lattice were obtained by least-squares fitting of 25 well-centered reflections in the range $30 \le 2\theta \le 40°$. The unit cell dimensions and symmetry were confirmed by axial photography. Intensity measurements were carried out at ambient temperature using a $\theta-2\theta$ scan technique. A total of 4715 data were collected. The intensities of three representative reflections were measured at regular intervals and revealed that no decay had occurred during data collection. An absorption correction based on azimuthal scans of several reflections near $\chi = 90°$ was applied to data. After equivalent reflections ($R_{merge} = 0.038$) were averaged, a total of 4466 data in the range $4 \le 2\theta \le 42$ remained. Of these, 3034 were considered observed with $F_o^2 > 2\sigma(F_o^2)$. Examination of systematic absences led to the selection of $P2_1/n$ as the space group. The positions of the metal atoms were determined through the use of the Patterson technique. The locations of subsequent non-hydrogen atoms were determined through a series of least-squares cycles and difference maps.

(11) Sheldrick, G. M. SHELXS-86; Institut für Anorganische Chemie der Universität Göttingen, Göttingen, FRG, 1986.

(12) The extinction parameter *x* is refined by least-squares, where F_c is multiplied by $k[1 + 0.001(x)(F_c^2)(\lambda)^3/\sin(2\theta)]^{-1/4}$; *k* = overall scale factor.

(13) Flack, H. D. *Acta Crystallogr.* **1983**, *A37*, 22.

(14) *R* factors based on F^2 are statistically about twice as large as those based on *F*, and an *R*-index based on all data is inevitably larger than one based only on data with *F* greater than a given threshold.

Hydrogen atoms were placed at calculated positions and allowed to ride on the associated carbon atom. All non-hydrogen atoms were refined using anisotropic displacement parameters. Final refinement of 442 parameters converged with residuals R (based on F) and R_w (based on F^2) of 0.049 and 0.124, respectively. The quality-of-fit based on F^2 for all data was 1.02 and the highest remaining peak in the final difference map, which was located 1.2 Å from Tc(1), was 0.79 e/Å^3.

$[Tc_2Cl_4(PMe_2Ph)_4][PF_6]\cdot{}^1/_2THF$ ($1\cdot{}^1/_2THF$). Single crystals of $1\cdot{}^1/_2$THF suitable for X-ray diffraction studies were obtained by addition of a 4:1 mixture of diethyl ether and THF to a solution of **1** in acetonitrile. The resulting saturated solution was cooled to −40 °C for a period of several days, producing a crop of green crystals. An acicular crystal with the approximate dimensions of 0.4 × 0.15 × 0.1 mm^3 was selected and attached to the tip of a glass fiber with epoxy cement. Intensity measurements were performed at ambient temperature on a Rigaku AFC5R diffractometer equipped with a rotating Cu radiation source ($\lambda_{Cu\ K\alpha}$ = 1.541 84 Å). A unit cell with parameters matching those of a primitive monoclinic lattice was obtained following least-squares refinement of 25 carefully centered reflections in the range $60 \le 2\theta \le 90°$. The cell dimensions and symmetry were confirmed by axial photography. Data collection was performed using a $\theta-2\theta$ scan motion. A total of 6089 data was collected over the range $5 \le 2\theta \le 110°$. After equivalent reflections (R_{merge} = 0.023) were averaged, a total of 5726 unique reflections remained, of which 4719 were considered observed with $F_o^2 > 2\sigma(F_o^2)$. The intensities of three representative reflections were monitored at regular intervals and revealed a loss of 9% in intensity over the course of the experiment. A linear decay correction was applied to the data to account for the loss in diffraction intensity. An empirical absorption correction was applied on the basis of azimuthal scans of several reflections with an Eulerian angle χ near 90°. The positions of the Tc atoms were determined using the Patterson method. The remaining non-hydrogen atoms were located from a series of alternating least-squares cycles and difference maps. All non-hydrogen atoms were refined with anisotropic displacement parameters. Hydrogen atoms were included in the structure factor calculation at idealized positions and were allowed to ride on the associated carbon atom. The $[PF_6]^-$ anion exhibited a disorder about the F(1)−P(5)−F(2) axis, resulting in the presence of two sets of four partially occupied F atoms in the equatorial plane. The anisotropic displacement parameters for these F atoms were restrained to be equivalent, and the occupancies of the two sets were refined, giving values of 60(2) and 40(2)% for the two orientations. The partially occupied interstitial THF molecule was also disordered over two different sites. The anisotropic thermal and geometric displacement parameters of the two orientations were restrained to be similar, and their occupancies were refined, giving values of 27(1) and 23(1)%. Final least-squares refinement of 570 parameters yielded residuals R (based on F) and R_w (based on F^2) of 0.050 and 0.141, respectively. A quality-of-fit of 1.08 based on all data was obtained. The largest remaining peak in the final difference map was 0.67 e/Å^3 and was associated with Tc(1).

$Tc_2Cl_5(PMe_2Ph)_3$ (2). Large, orange, block-shaped crystals of **2** were obtained by slow evaporation of a solution of **2** in CH_2Cl_2 and heptane. A well-shaped single crystal with the approximate dimensions of 0.4 × 0.3 × 0.3 mm^3 was selected and mounted with epoxy cement onto the tip of a glass fiber. Intensity measurements were made at ambient temperature on an Enraf-Nonius CAD4 diffractometer equipped with graphite monochromated Mo radiation ($\lambda_{Mo\ K\alpha}$ = 0.71073 Å). Indexing and least-squares refinement of 25 well-centered reflections in the range $40 \le 2\theta \le 50°$ yielded lattice parameters consistent with a primitive monoclinic cell. The lattice parameters and symmetry were confirmed via axial photography. Using a $\theta-2\theta$ scan technique, a total of 5722 data were collected in the range $4 \le 2\theta \le 50°$. Averaging of equivalent reflections left 5424 unique reflections, of which 4243 were considered observed with $F_o^2 > 2\sigma(F_o^2)$. Routine monitoring of three standard reflections revealed a 2% decay in intensity that was accounted for by a linear decay correction. An absorption correction was applied on the basis of azimuthal scans of several reflections near χ = 90°. Careful examination of the systematic absences led to the selection of the space group $P2_1/c$. The positions of the Tc, Cl, and P atoms were determined by the Patterson method. The remaining non-hydrogen atoms were subsequently located by an alternating series of least-squares cycles and Fourier difference maps. Hydrogen atoms were initially placed at calculated positions but were allowed to fully refine with isotropic displacement parameters. All non-hydrogen atoms were refined with anisotropic displacement parameters. After initial anisotropic refinement, it was apparent that two additional orientations of the Tc_2 unit were present perpendicular to the Tc(1)−Tc(2) bond. The thermal displacement parameters of the Tc atoms and Tc−Tc bond lengths were restrained to be similar, and the occupancies of the three mutually perpendicular Tc_2 units were refined. Anisotropic refinement converged with occupancies for the three orientations of 96.7(1), 1.81(8), and 1.46(8)%. Final least-squares refinement of 478 parameters produced residuals R (based on F) and R_w (based on F^2) of 0.026 and 0.066, respectively. The largest remaining peak in the difference map was 0.39 e/Å^3, and the quality-of-fit based on F^2 for all data was 1.10.

Results and Discussion

Synthesis. Previously we demonstrated that ditechnetium complexes of the type $Tc_2Cl_4(PR_3)_4$ exhibit two reversible one-electron-oxidation processes consistent with a $\sigma^2\pi^4\delta^2\delta^{*2}$ ground state electronic configuration.[1a] In the case of $Tc_2Cl_4(PMe_2Ph)_4$, the first oxidation process is readily accessible, occurring at $E_{1/2}$ = −0.26 V vs ferrocene, whereas the second oxidation, which appears at $E_{1/2}$ = 0.92 V, is much less accessible. As anticipated on the basis of our electrochemical studies, $Tc_2Cl_4(PMe_2Ph)_4$ readily undergoes a one-electron oxidation using $[Cp_2Fe]^+$ as an oxidant. Slow addition of $[Cp_2Fe][PF_6]$ to a stirred suspension of $Tc_2Cl_4(PMe_2Ph)_4$ in acetonitrile produced a dark green solution from which the mixed-valent species $[Tc_2Cl_4(PMe_2Ph)_4][PF_6]$ (**1**) was isolated in approximately 80% yield (eq 1). On the basis of elemental analysis and X-ray crystallography, inclusion of THF in the work-up procedure results in a crystalline form of **1** that contains half of a molecule of THF per dinuclear cation. $[NO][PF_6]$ was also used as an oxidant, but the reaction was complicated by the formation of other unidentified byproducts.

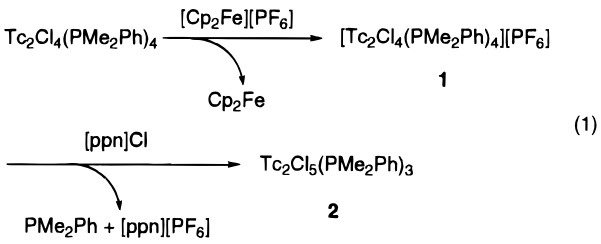

(1)

When oxidation of $Tc_2Cl_4(PMe_2Ph)_4$ is performed in the presence of Cl^- ion, the neutral Tc(II)−Tc(III) species $Tc_2Cl_5(PMe_2Ph)_3$ is produced in high yield. The formation of $Tc_2Cl_5(PMe_2Ph)_3$ occurs when the one-electron oxidation is followed by substitution of Cl^- for a phosphine ligand. Consistent with the proposed two-step pathway, addition of ppnCl to a solution of $[Tc_2Cl_4(PMe_2Ph)_4]^+$ yields $Tc_2Cl_5(PMe_2Ph)_3$. Indeed, the method recommended here involves initial oxidation of $Tc_2Cl_4(PMe_2Ph)_4$ to produce a green solution of $[Tc_2Cl_4(PMe_2Ph)_4]^+$ that is then treated with halide ion to give $Tc_2Cl_5(PMe_2Ph)_3$ as an orange precipitate (eq 1). The transformation of $[Tc_2Cl_4(PMe_2Ph)_4]^+$ to $Tc_2Cl_5(PMe_2Ph)_3$ is nearly quantitative, as evidenced by the high isolated yield obtained for **2**. Electrochemical studies further demonstrate that addition of Cl^- to a solution of **1** results in nearly quantitative formation of **2**. The substitution reaction of $[Tc_2Cl_4(Me_2Ph)_4]^+$ is favored by the reduction of the overall charge on the molecule that occurs upon replacement of a neutral phosphine donor by a chloride ligand. Similar coupled electrochemical−chemical (EC) type pathways have been demonstrated for the formation

Table 6. Spectroscopic and Electrochemical Data for $[Tc_2Cl_4(PMe_2Ph)_4][PF_6]$ (**1**) and $Tc_2Cl_5(PMe_2Ph)_3$ (**2**)

	1	**2**
electronic absorption spectrum[a]		
λ_{max}, nm (ϵ, M^{-1} cm^{-1})	1417 (2150), 586 (350), 467 (340)	1405 (1950), 728 (30) 520 (280), 445 (1250), 395 (850)
EPR spectrum[b]		
g (A, $\times 10^{-4}$ cm^{-1})	$g_\perp$ ($\|A_\perp\|$): 2.03 (133) $g_{\|\|}$ ($\|A_{\|\|}\|$): 1.95 (146)	g_1 ($\|A_1\|$): 2.31 (113) g_2 ($\|A_2\|$): 2.23 (81) g_3 ($\|A_3\|$): 1.75 (83)
cyclic voltammetry potentials[a,c]		
$E_{1/2,ox}$, V vs Cp_2Fe	0.92	0.53
$E_{1/2,red}$, V vs Cp_2Fe	−0.26	−0.74

[a] Solution measurements were performed in CH_3CN for **1** and CH_2Cl_2 for **2**. [b] EPR spectral data for **1** were obtained at 70 K as a frozen acetonitrile/toluene solution. Spectral data for **2** were obtained at 50 K as a frozen dichloromethane/toluene solution. The values for g and the associated hyperfine coupling constants $|A|$ are estimated. [c] Measured using 0.1 M $[Bu_4N][PF_6]$ as a supporting electrolyte at a scan rate of 200 mV s^{-1} using a Pt disk electrode.

of $Re_2Cl_5(PR_3)_3$ and $Re_2Cl_6(PR_3)_2$ in electrochemically oxidized solutions of $Re_2Cl_4(PR_3)_4$ in the presence of Cl^- ion.[15]

Spectroscopy. Spectroscopic and electrochemical data for **1** and **2** are presented in Table 6. Both $[Tc_2Cl_4(PMe_2Ph)_4][PF_6]$ and $Tc_2Cl_5(PMe_2Ph)_3$ display IR bands associated with the coordinated PMe_2Ph ligand. Complex **1** also exhibits a strong band at 834 cm^{-1} attributed to the ν(P−F) mode of the $[PF_6]^-$ counter ion. The electronic spectrum of $[Tc_2Cl_4(PMe_2Ph)_4][PF_6]$ in acetonitrile reveals a strong, broad absorption in the near-IR at 1418 nm that is characteristic of a M_2^{5+} core possessing a $\sigma^2\pi^4\delta^2\delta^*$ ground state electronic configuration.[15,16] This band is readily assigned to an allowed $\delta \rightarrow \delta^*$ transition that was unavailable prior to removal of an electron from the δ^* orbital.[17] Some vibrational fine structure resulting from coupling with the Tc−Tc stretching mode is discernible at room temperature. While an accurate measure of the excited state Tc−Tc stretching frequency is not possible because of the broadness of the absorption band, the ν(Tc−Tc) vibrational progression is estimated to be 350 ± 20 cm^{-1}. This value is in general agreement with those obtained for other metal−metal multiply-bonded complexes of Mo and Tc.[18] Higher energy transitions are also present at 586 and 467 nm. Likewise, in accordance with its predicted $\sigma^2\pi^4\delta^2\delta^*$ ground state electronic configuration, $Tc_2Cl_5(PMe_2Ph)_3$ also exhibits a $\delta \rightarrow \delta^*$ transition in the near-IR region. This broad and relatively intense absorption appears at 1405 nm. No vibronic fine structure is observed at room temperature. Several higher energy absorptions are also present at 728, 520, 445, 395, and 342 nm.

The energy of these $\delta-\delta^*$ transitions, *ca.* 7100 cm^{-1}, may be compared with those in the analogous Re species,[19] which are at slightly lower energy, *ca.* 6600 cm^{-1}. In the $[Tc_2Cl_8]^{3-}$ ion, the transition is at a still lower energy,[19] *ca.* 6250 cm^{-1}.

Confirmation for the paramagnetism of **1** and **2** was provided by EPR spectroscopy. The X-band EPR spectrum of $[Tc_2Cl_4(PMe_2Ph)_4][PF_6]$, which was obtained from a frozen CH_3CN/toluene solution recorded at 70 K (Figure 1a), exhibits the qualitative features anticipated for an axially symmetric $S = {}^1/_2$ spin system with anisotropic hyperfine coupling to two equivalent ^{99}Tc ($I = {}^9/_2$) nuclei. A series of broad bands, consisting of parallel and perpendicular orientation lines, appear from 2060 to 4760 G. Hyperfine coupling of the unpaired spin to two equivalent, $I = {}^9/_2$ nuclei should produce 19 lines each for the perpendicular and parallel orientations. The broadness of the lines is partially attributed to further coupling to four equivalent ^{31}P nuclei ($I = {}^1/_2$), which will further split each individual line into a quintet. The position of the 10th line counting from the lowest field line was used to obtain a value of 2.03 for $g_\perp$. The anisotropic hyperfine coupling constant, $|A_\perp|$, was estimated to be 133 × 10^{-4} cm^{-1} from the splitting of the nine lowest field lines. Likewise, $g_{||}$ was estimated to be 1.95 from the position of the 10th line counting from higher field. The splitting of the equidistant high-field lines was used to obtain a value of 146 × 10^{-4} cm^{-1} for $|A_{||}|$.

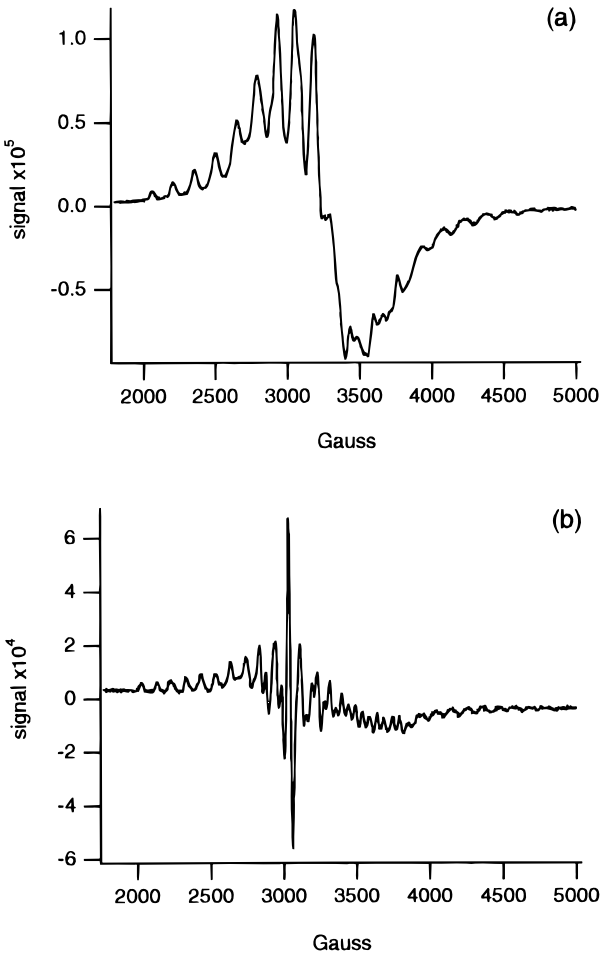

Figure 1. EPR spectra of (a) $[Tc_2Cl_4(PMe_2Ph)_4][PF_6]$ at 70 K in a 1:1 mixture of acetonitrile/toluene and (b) $Tc_2Cl_5(PMe_2Ph)_3$ at 50 K in a 1:1 mixture of methylene chloride/toluene.

The EPR spectrum of $Tc_2Cl_5(PMe_2Ph)_3$ at 50 K, measured as a frozen solution in a mixture of CH_2Cl_2 and toluene, is presented in Figure 1b. The spectrum exhibits a complex series of lines ranging from 2030 to 4850 G. The spectrum may be

(15) (a) Brant, P.; Salmon, D. J.; Walton, R. A. *J. Am. Chem. Soc.* **1978**, *100*, 4424. (b) Dunbar, K. R.; Walton, R. A. *Inorg. Chem.* **1985**, *24*, 5.
(16) (a) Ebner, J. R.; Walton, R. A. *Inorg. Chim. Acta* **1975**, *14*, L45. (b) Cotton, F. A.; Fanwick, P. E.; Gage, L. D.; Kalbacher, B.; Martin, D. S. *J. Am. Chem. Soc.* **1977**, *99*, 5642.
(17) Bursten, B. E.; Cotton, F. A.; Fanwick, P. E.; Stanley, G. G.; Walton, R. A. *J. Am. Chem. Soc.* **1983**, *105*, 2606.
(18) See: Reference 3; p 739.
(19) See: Reference 3; pp 701−702.

interpreted as a rhombic, $S = {}^1/_2$ system with the lines belonging to three mutually perpendicular **g** tensors and anisotropic hyperfine coupling to two inequivalent ^{99}Tc nuclei. The anistropy of the spectrum is not surprising considering the low molecular symmetry of the molecule (C_s symmetry as opposed to D_{2d} for **1**). However, from the equidistant spacing of the 10 lines at the highest and lowest fields, we conclude that the individual ^{99}Tc coupling constants are similar in magnitude, and therefore only a 19 line pattern is expected for each **g** tensor despite the inequivalency of the ^{99}Tc nuclei. The g_1 value, estimated from the nine lines at lowest field, is 2.31 with $|A_1| = 113 \times 10^{-4}$ cm^{-1}. On the basis of the 10 broad lines at high field, g_3 was estimated to be 1.75 with an anisotropic coupling constant, $|A_3|$, of 83×10^{-4} cm^{-1}. The intense line at 3048 G was assigned as g_2, providing a value of 2.23 with the hyperfine coupling constant $|A_3|$ estimated to be 81×10^{-4} cm^{-1}.

Qualitatively, the EPR spectra of $[Tc_2Cl_4(PMe_2Ph)_4][PF_6]$ and $Tc_2Cl_5(PMe_2Ph)_3$ are similar to those documented for other M_2^{5+} (M = Tc, Re) complexes.[3] Despite the higher nuclear spin of ^{99}Tc, the EPR spectra of **1** and **2** appear less complicated and better resolved than the corresponding spectra of the analogous Re complexes. The reasons for this are 2-fold. Firstly, rhenium exists as a mixture of two naturally occurring $I = {}^5/_2$ isotopes, ^{185}Re and ^{187}Re,[20] whereas technetium is isotopically pure ^{99}Tc with $I = {}^9/_2$. Secondly, the anisotropic hyperfine coupling constants for Re are greater than those for Tc. Consequently, the lines corresponding to the separate **g** tensors tend to overlap more, producing a more complicated spectrum. The **g** values and Tc hypefine coupling constants found for **1** and **2** are similar to those obtained for $Y[Tc_2Cl_8]\cdot 9H_2O$.[4,21] The observation that $g_{\|} < 2$, $g_{\perp} > 2$, and $g_{av} \geq 2$ supports the assignment of the unpaired electron to the Tc−Tc δ^* molecular orbital.[21]

Molecular Structures. $[Tc_2Cl_4(PMe_2Ph)_4][PF_6]$ was crystallized in three different structural forms; an orthorhombic polymorph (**1a**), a monoclinic polymorph (**1b**), and a monoclinic form that contained a THF of crystallization for every two formula units of $[Tc_2Cl_4(PMe_2Ph)_4][PF_6]$. Selected bond distances and angles for compounds **1a**, **1b**, **1**·$^1/_2$THF are listed in Table 7. Crystalline **1**·$^1/_2$THF is isomorphous with the analogous Re complex $[Re_2Cl_4(PMe_2Ph)_4][PF_6]\cdot {}^1/_2$THF.[22] The Tc−Tc bond in polymorph **1a** lies perpendicular to a crystallographic two-fold axis, making only half of the molecule unique. In contrast, the cations in **1b** and **1**·$^1/_2$THF crystallize without any imposed symmetry. An ORTEP diagram of the dinuclear cation in **1b** is presented in Figure 2 and is representative of all three forms. X-ray crystallographic studies show that in each structure the dinuclear cation adopts an eclipsed $M_2X_4L_4$ geometry with a 1,3,6,8 arrangement of ligands, similar to that observed for the neutral complex $Tc_2Cl_4(PMe_2Ph)_4$. The two *trans*-$TcCl_2P_2$ fragments are rotated 90° from each other, resulting in D_{2d} symmetry for the inner $Tc_2Cl_4P_4$ core in all three forms of **1**. The eclipsed nature of the dinuclear cations is readily apparent by examination of the mean torsion angles about the metal−metal bond. The average torsion angles are 2.07[3], 0.4[8], and 1.1[7]° for **1a**, **1b**, **1**·$^1/_2$THF. The average Tc−Tc bond length for the three structural forms of **1** is 2.1074[9] Å. The mean length is 0.02 Å shorter than that determined for $Tc_2Cl_4(PMe_2Ph)_4$, consistent with an increase in the formal bond order from 3 to 3.5 due to the depopulation of a δ^* orbital. Similar bond distance changes were observed upon oxidation of the analogous $Re_2Cl_4(PMe_2Ph)_4$ complex.[22] As has been noted previously, two countervailing factors must be taken into consideration when examining bond distance changes upon oxidation or reduction of dimetal cores.[3] Intuitively, an increase in bond order is expected to shorten the metal−metal separation, with changes in the occupation of σ- and π-type orbitals producing more dramatic variations. However, the effect of increased formal charge on the metal atoms tends to weaken σ and π metal−metal bonding interactions through contraction of the metal d-orbitals, which tends to cause a slight lengthening of the metal−metal bond. For example, although an increase in formal bond order from 3.5 to 4.0 is observed in going from $[Tc_2Cl_8]^{3-}$ to $[Tc_2Cl_8]^{2-}$, the Tc−Tc bond length decreases by only *ca.* 0.04 Å because of the influence of the increased formal charge

Table 7. Selected Bond Lengths and Angles (deg) for $[Tc_2Cl_4(PMe_2Ph)_4][PF_6]$ (**1a**), $[Tc_2Cl_4(PMe_2Ph)_4][PF_6]$ (**1b**), and $[Tc_2Cl_4(PMe_2Ph)_4][PF_6]\cdot {}^1/_2$THF (**1**·$^1/_2$THF)

Lengths

	1a[a]	**1b**	**1**·$^1/_2$THF
Tc−Tc	2.1092(9)	2.106(1)	2.1073(8)
Tc(1)−Cl(1)	2.339(2)	2.339(3)	2.331(2)
Tc(1)−Cl(2)	2.322(2)	2.331(3)	2.336(2)
Tc(1)−P(1)	2.483(2)	2.487(3)	2.489(2)
Tc(1)−P(2)	2.488(2)	2.490(3)	2.481(2)
Tc(2)−Cl(3)		2.342(3)	2.330(2)
Tc(2)−Cl(4)		2.331(3)	2.329(2)
Tc(2)−P(3)		2.480(3)	2.476(2)
Tc(2)−P(4)		2.494(3)	2.485(2)

Angles

	1a[a]	**1b**	**1**·$^1/_2$THF
Tc−Tc(1)−Cl(1)	108.60(6)	108.54(8)	109.96(6)
Tc−Tc(1)−Cl(2)	108.24(6)	107.34(8)	108.10(6)
Tc−Tc(1)−P(1)	105.96(6)	106.44(7)	106.06(6)
Tc−Tc(1)−P(2)	106.62(5)	105.27(8)	105.07(6)
Cl(1)−Tc(1)−Cl(2)	143.17(8)	144.1(1)	141.92(7)
Cl(1)−Tc(1)−P(1)	84.88(6)	83.90(9)	83.10(7)
Cl(1)−Tc(1)−P(2)	84.96(8)	86.4(1)	85.69(7)
Cl(2)−Tc(1)−P(1)	84.97(8)	85.9(1)	85.40(7)
Cl(2)−Tc(1)−P(2)	84.85(7)	84.4(1)	85.74(7)
P(1)−Tc(1)−P(2)	147.42(7)	148.3(1)	148.85(7)
Tc(1)−Tc(2)−Cl(3)		106.45(8)	107.98(6)
Tc(1)−Tc(2)−Cl(4)		110.09(8)	108.89(6)
Tc(1)−Tc(2)−P(3)		106.29(8)	107.08(6)
Tc(1)−Tc(2)−P(4)		107.12(8)	106.04(6)
Cl(3)−Tc(2)−Cl(4)		143.5(1)	143.12(8)
Cl(3)−Tc(2)−P(3)		84.94(9)	85.54(7)
Cl(3)−Tc(2)−P(4)		87.6(1)	83.88(7)
Cl(4)−Tc(2)−P(3)		84.63(9)	83.04(8)
Cl(4)−Tc(2)−P(4)		82.21(9)	86.86(8)
P(3)−Tc(2)−P(4)		146.5(1)	146.87(7)

[a] The dinuclear cation resides on a crystallographic 2-fold axis; therefore, only half of the molecular unit is unique.

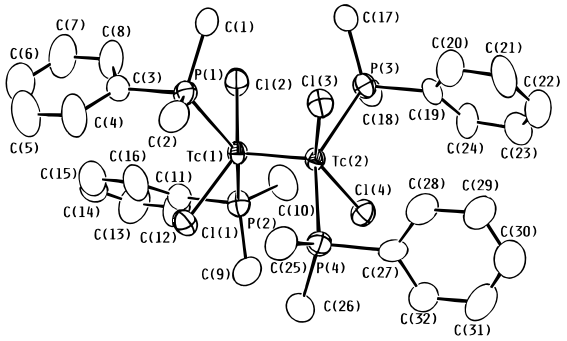

Figure 2. ORTEP drawing depicting the $[Tc_2Cl_4(PMe_2Ph)_4]^+$ cation in polymorph **1b**. Thermal ellipsoids are drawn at the 40% probability level. Hydrogen atoms have been omitted for clarity.

(20) Cotton, F. A.; Pedersen, E. *J. Am. Chem. Soc.* **1975**, *97*, 303.
(21) Cotton, F. A.; Pedersen, E. *Inorg. Chem.* **1975**, *14*, 383.
(22) Cotton, F. A.; Dunbar, K. R.; Falvello, L. R.; Tomas, M.; Walton, R. A. *J. Am. Chem. Soc.* **1983**, *105*, 4950.

on the metal centers.[23] In the present case, the increase in bond order offsets any bond lengthening resulting from the increased charge on the dinuclear core. The changes in technetium−ligand bond distances upon oxidation of $Tc_2Cl_4(PMe_2Ph)_4$ follow the same trends observed in the analogous dirhenium system. Thus, the average Tc−Cl bond length decreases by 0.06 Å from 2.394[2] to 2.333[2] Å upon oxidation, while the average Tc−P bond undergoes a slight increase in length from 2.45[1] to 2.485-[2] Å.

In contrast to the structure of $Tc_2Cl_4(PMe_2Ph)_4$, none of the three structures of **1** show any indication of disorder of the Tc_2 core within the ligand cage. In all three structures, the phenyl rings of the phosphine ligands are directed away from the Tc_2 unit and lie parallel to the metal−metal bond. The same disposition of the phenyl groups was previously observed for the primary orientation of the Tc−Tc bond in the structure of $Tc_2Cl_4(PMe_2Ph)_4$. While one might have expected the $[PF_6]^-$ anions to exert an attractive Coulombic force on the positively charged dimetal units which orients the Tc−Tc axis in a single direction,[24] an examination of the packing diagrams for all three polymorphs reveals that the $[PF_6]^-$ counter anion is not necessarily aligned with the faces of the quasi-cube that contains the Tc atoms. In fact, the anions in **1a** and **1**·$^1/_2$THF are directed toward the corners of the quasi-cube of ligands and not the faces. Only in the structure of **1b** is the $[PF_6]^-$ anion collinear with the metal−metal vector (Tc(2)−Tc(1)- - -P(5) = 172.04(2)°). Moreover, the distances between the Tc atoms and the P atom of the counter anion are greater than 7.5 Å. Therefore, the resulting consequences of any Coulombic attractions at this distance will be negligible. A more plausible explanation for the ordering observed in the structure of **1** can be found in the relative energies of the different conformational isomers formed by the disordering of the Tc−Tc unit within the quasi-cube of ligands. As was previously noted in the structure of $Tc_2Cl_4(PMe_2Ph)_4$, any disordering of the Tc_2 unit creates a conformational isomer in which the Tc−Tc bond is perpendicular to the phenyl rings of the phosphine ligands rather than parallel, as in the present case. Apparently, the minor structural changes that occur upon oxidation sufficiently destabilize the conformations in which the Tc_2 unit is perpendicular to the phenyl groups, thereby favoring the formation of a single conformational isomer. A similar phenomenon was observed in the crystal structures of $[Re_2Cl_4(PMe_2Ph)_4]^{n+}$ ($n = 0, 1, 2$).[22]

$Tc_2Cl_5(PMe_2Ph)_3$ is structurally similar to $Tc_2Cl_4(PMe_2Ph)_4$ and $[Tc_2Cl_4(PMe_2Ph)_4]^+$ in that it consists of two eclipsed ML_4 fragments with a relatively short Tc−Tc separation. However, one of the phosphine ligands has been replaced by a Cl^- ion (Figure 3), leaving the PMe_2Ph ligands in a 1,3,6 arrangement. Important geometric parameters for **2** are presented in Table 8. The 1,3,6-structural isomer is the most sterically favored in which the phosphine ligands that are coordinated to the same Tc atom are *trans* to each other. Unlike **1**, the Tc_2 core in **2** is disordered within the quasi-cube of phosphine and chloride ligands, giving rise to three mutually perpendicular orientations (Figure 4). This disorder is not crystallographically imposed, as the dinuclear cation resides on a general position within the unit cell. One orientation is predominant with a refined occupancy of 96.7(1)%. The other two minor orientations are present at 1.81(8) and 1.46(8)% occupancies. Derived structural parameters involving the minor Tc orientations are available as Supplementary Information. Since all of the phosphines reside at nonadjacent corners described by the quasi-cube of ligands, each of the three orientations within this cube produces a 1,3,6-isomer of $Tc_2Cl_5(PMe_2Ph)_3$. However, these isomers are not conformationally equivalent. Just as was observed for the structure of $Tc_2Cl_4(PMe_2Ph)_4$, each orientation produces a conformational isomer that differs by the orientation of the PMe_2Ph ligand with respect to the Tc−Tc bond and the chloride ligands.[1a] Again, the primary orientation of the Tc_2 unit is directed parallel with the phenyl rings of the phosphine ligand, as was observed for the structures of $Tc_2Cl_4(PMe_2Ph)_4$ and $[Tc_2Cl_4(PMe_2Ph)_4][PF_6]$. For the minor orientations, the phosphine phenyl rings lie perpendicular to the metal−metal bond. In solution, these isomers may readily interconvert by rotation about the Tc−P bonds.

The Tc−Tc bond length of 2.1092(4) Å for the primary orientation for $Tc_2Cl_5(PMe_2Ph)_3$ is consistent with the presence

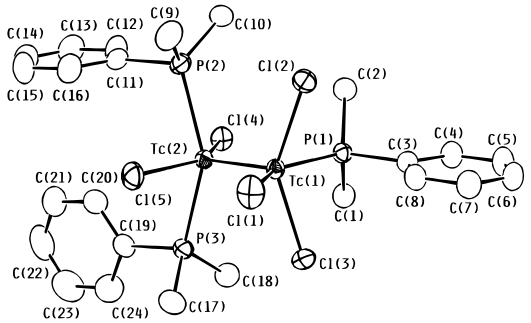

Figure 3. ORTEP plot of $Tc_2Cl_5(PMe_2Ph)_3$ (**2**) showing only the primary orientation of the Tc_2 unit. Thermal ellipsoids are shown at the 40% probability level. Hydrogen atoms have been omitted for clarity.

Table 8. Selected Bond Distances (Å) and Angles (deg) for $Tc_2Cl_5(PMe_2Ph)_3$ (**2**)[a]

Tc(1)−Tc(2)	2.1092(4)	Tc(1)−Cl(1)	2.3406(9)
Tc(1)−Cl(2)	2.3465(8)	Tc(1)−Cl(3)	2.3359(9)
Tc(1)−P(1)	2.4647(9)	Tc(2)−Cl(4)	2.3555(9)
Tc(2)−Cl(5)	2.3415(9)	Tc(2)−P(2)	2.4679(9)
Tc(2)−P(3)	2.4808(9)		
Tc(2)−Tc(1)−Cl(1)	106.00(3)	Tc(1)−Tc(2)−Cl(4)	111.23(2)
Tc(2)−Tc(1)−Cl(2)	108.65(2)	Tc(1)−Tc(2)−Cl(5)	105.27(3)
Tc(2)−Tc(1)−Cl(3)	108.21(2)	Tc(1)−Tc(2)−P(2)	104.19(2)
Tc(2)−Tc(1)−P(1)	103.89(2)	Tc(1)−Tc(2)−P(3)	104.63(2)
Cl(1)−Tc(1)−Cl(2)	88.00(4)	Cl(4)−Tc(2)−Cl(5)	143.50(3)
Cl(1)−Tc(1)−Cl(3)	87.82(4)	Cl(4)−Tc(2)−P(2)	86.87(3)
Cl(2)−Tc(1)−Cl(3)	142.61(3)	Cl(4)−Tc(2)−P(3)	86.83(3)
Cl(1)−Tc(1)−P(1)	150.10(3)	Cl(5)−Tc(2)−P(2)	84.52(3)
Cl(2)−Tc(1)−P(1)	82.90(3)	Cl(5)−Tc(2)−P(3)	83.78(3)
Cl(3)−Tc(1)−P(1)	82.50(3)	P(2)−Tc(2)−P(3)	150.85(3)

[a] Bond distances and angles involving the minor disordered Tc atoms are presented in the supplementary material.

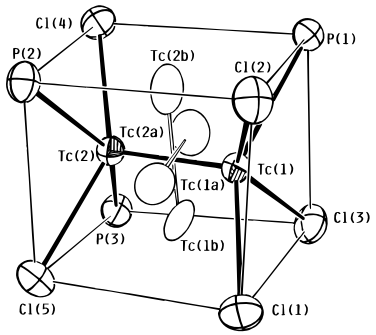

Figure 4. ORTEP drawing of **2** illustrating the three orientations of the Tc−Tc bond within the quasi-cube of PMe_2Ph and Cl^- ligands.

(23) (a) Cotton, F. A.; Daniels, L.; Davison, A; Orvig, C. *Inorg. Chem.* **1981**, *20*, 3051. (b) Cotton, F. A.; Davison, A.; Day, V. W.; Fredrich, M. F.; Orvig, C.; Swanson, R. *Inorg. Chem.* **1982**, *21*, 1211.

(24) Repulsive interactions between cations and M_2 units has been shown to influence the orientation of the M−M bond within the quasi-cube of ligands. Cotton, F. A.; Matonic, M. H.; Silva, D. O. *Inorg. Chim. Acta* **1995**, *234*, 115.

of a Tc−Tc multiple bond. Despite the substitution of a Cl^- for a phosphine ligand, the metal−metal bond distance remained essentially unchanged relative to **1**. The steric influence of the phosphine ligands manifests itself in the Tc−Tc−Cl bond angles. For Cl(4), which is situated opposite a phosphine ligand on Tc(1), the Tc(1)−Tc(2)−Cl(4) angle is 5.96° greater than the corresponding angle for Cl(5), which lies opposite Cl(1). Surprisingly, the Tc−Cl distances do not exhibit the expected trans influence exerted by the phosphine ligands. The Tc(1)−Cl(1) bond distance is intermediate among those observed for the other four Tc−Cl bonds. A *trans* influence on the M−Cl bond length has been observed in the structures of several $Re_2Cl_x(PR_3)_{8-x}$ ($x = 5-7$) type compounds.[25] One factor that contributes to the lack of an observable *trans* influence in the structure of **2** is the presence of disorder in the orientation of the Tc−Tc bond. The anticipated variations in bond length resulting from a *trans* influence are relatively small (*ca.* 0.02 Å) and are likely masked by the disorder of the dimetal units. By way of an example, the structure of 1,3,6−$W_2Cl_5(PMe_3)_3$, which has a 1.8% disordering of the W_2 core, also does not exhibit a trans-influence, yet the structure of 1,3,6−$Re_2Cl_5(PMe_3)_3$, which has an ordered Re−Re bond, shows an elongation of the Re−Cl bond *trans* to the PMe_3 ligand of about 0.02 Å.[26,27]

Electrochemistry. The cyclic voltammogram of $[Tc_2Cl_4(PMe_2Ph)_4][PF_6]$ reveals two reversible one-electron redox processes at the same potentials as those observed for the parent complex $Tc_2Cl_4(PMe_2Ph)_4$. However, instead of these couples corresponding to successive one-electron oxidation processes, these redox couples now represent one-electron oxidation and reduction processes. The similarity of the cyclic voltammograms of $[Tc_2Cl_4(PMe_2Ph)_4]^+$ and $Tc_2Cl_4(PMe_2Ph)_4$ indicated that no structural rearrangement occurred upon oxidation and the metal−metal bond remained intact, as later confirmed by X-ray crystallography (*vide supra*). Likewise, a cyclic voltammogram of $Tc_2Cl_5(PMe_2Ph)_3$ reveals that two reversible redox processes are available. A reduction couple appears at −0.74 V vs Cp_2Fe, and a one-electron-oxidation process is present at +0.53 V vs Cp_2Fe. As a result of the replacement of a π-donating Cl^- ion for a phosphine ligand, both redox processes occur at more negative potentials than those observed for $[Tc_2Cl_4(PMe_2Ph)_4]^+$.

The results from the electrochemical study further support the assignment of a $\sigma^2\pi^4\delta^2\delta^*$ ground state electronic configuration for compounds **1** and **2**. The occurrence of accessible oxidation and reduction processes correlates well with the observed electrochemical properties of other mixed halide−phosphine complexes of Re_2^{5+} that possess the same electronic ground state.[15,22,26] Moreover, the reversibility of the redox couples suggests that subsequent addition or removal of an electron from the Tc_2^{5+} cores of **1** and **2** does not induce a major structural change. The preparation of **1** and **2** from $Tc_2Cl_4(PMe_2Ph)_4$ illustrates that both the Tc_2^{4+} and Tc_2^{5+} cores can be stabilized by a mixed halide−phosphine ligand environment. Unfortunately, although the accessibility of the Tc_2^{6+} core has been demonstrated by cyclic voltammetry, we have not successfully isolated a mixed halide−phosphine complex possessing a Tc−Tc quadruple bond by chemical oxidation of **1** or **2**.

Acknowledgment. This work was supported by the Laboratory Directed Research and Development Program at Los Alamos National Laboratory. The authors also acknowledge financial assistance from the National Science Foundation and the Laboratory for Molecular Structure and Bonding for support of the facilities at Texas A&M University. We thank Dr. Robert Donahoe (Los Alamos National Laboratory) for assistance in obtaining EPR spectral data. The authors also thank Dr. Robert Hightower (Oak Ridge National Laboratory) for a generous gift of ammonium pertechnetate.

Supporting Information Available: Tables of crystallographic parameters, atomic positional and thermal parameters, complete bond distances and angles, and anisotropic thermal parameters and figures of ORTEP drawings of **1a** and **1**·$^1/_2$THF (31 pages). Ordering information is given on any current masthead page.

IC9508583

(25) (a) Cotton, F. A.; Vidyasagar, K. *Inorg. Chim. Acta* **1989**, *166*, 105. (b) Cotton, F. A.; Diebold, M. P.; Roth, W. J. *Inorg. Chim. Acta* **1988**, *144*, 17. (c) Ferry, J.; Gallagher, J.; Cunningham, D.; McArdle, P. *Inorg. Chim. Acta* **1989**, *164*, 185. (d) Ferry, J.; Gallagher, J.; Cunningham, D.; McArdle, P. *Inorg. Chim. Acta* **1990**, *172*, 79.
(26) Cotton, F. A.; Price, A.; Vidyasagar, K. *Inorg. Chem.* **1990**, *29*, 5143.
(27) Cotton, F. A.; Dikarev, E. V. *Inorg. Chem.* **1995**, *34*, 3809.